The Astrophysical Journal Letters, 914:L23 (7pp), 2021 June 10 https://doi.org/10.3847/2041-8213/ac024f

A Recently Quenched Isolated Dwarf Galaxy Outside of the Local Group Environment

Ava Polzin[1], Pieter van Dokkum[1], Shany Danieli[1,2,3,4,8], Johnny P. Greco[5,9], and Aaron J. Romanowsky[6,7]
[1] Department of Astronomy, Yale University, New Haven, CT 06511, USA; ava.polzin@yale.edu
[2] Department of Physics, Yale University, New Haven, CT 06520, USA
[3] Yale Center for Astronomy and Astrophysics, Yale University, New Haven, CT 06511, USA
[4] Institute for Advanced Study, 1 Einstein Drive, Princeton, NJ 08540, USA
[5] Center for Cosmology and AstroParticle Physics (CCAPP), The Ohio State University, Columbus, OH 43210, USA
[6] Department of Physics & Astronomy, One Washington Square, San José State University, San Jose, CA 95192, USA
[7] University of California Observatories, 1156 High Street, Santa Cruz, CA 95064, USA
Received 2021 March 22; revised 2021 May 14; accepted 2021 May 17; published 2021 June 15

Abstract

We report the serendipitous identification of a low-mass ($M_* \sim 2 \times 10^6\ M_\odot$), isolated, likely quenched dwarf galaxy in the "foreground" of the COSMOS-CANDELS field. From deep Hubble Space Telescope (HST) imaging we infer a surface brightness fluctuation distance for COSMOS-dw1 of $D_{\rm SBF} = 22 \pm 3$ Mpc, which is consistent with its radial velocity of $cz = 1222 \pm 64\ {\rm km\ s^{-1}}$ via Keck/LRIS. At this distance, the galaxy is 1.4 Mpc in projection from its nearest massive neighbor. We do not detect significant Hα emission (EW(Hα)$= -0.4 \pm 0.5$ Å), suggesting that COSMOS-dw1 is likely quenched. Very little is currently known about isolated quenched galaxies in this mass regime. Such galaxies are thought to be rare, as there is no obvious mechanism to permanently stop star formation in them; to date there are only four examples of well-studied quenched field dwarfs, only two of which appear to have quenched in isolation. COSMOS-dw1 is the first example outside of the immediate vicinity of the Local Group. COSMOS-dw1 has a relatively weak D_n4000 break and the HST data show a clump of blue stars indicating that star formation ceased only recently. We speculate that COSMOS-dw1 was quenched due to internal feedback, which was able to temporarily suspend star formation. In this scenario the expectation is that quenched isolated galaxies with masses $M_* = 10^6$–$10^7\ M_\odot$ generally have luminosity-weighted ages $\lesssim$1 Gyr.

Unified Astronomy Thesaurus concepts: Dwarf galaxies (416); Galaxy quenching (2040); Quenched galaxies (2016); Galaxy evolution (594)

1. Introduction

Dwarf galaxies in the Local Group play a pivotal role in many areas of astrophysics, including star formation, galaxy formation, and cosmology (see, e.g., Mateo 1998; Simon 2019). Given their outsized importance and impact there is great interest in finding dwarf galaxies at larger distances, as they provide information on the environmental dependence of low-mass galaxy formation and can be used to determine how typical Local Group galaxies are for the general population (Weisz et al. 2011a).

Most general galaxy catalogs are biased against the lowest-mass dwarfs due to incompleteness (e.g., Tollerud et al. 2008; Walsh et al. 2009), which is caused by their low surface brightness (see Danieli et al. 2018). To overcome this barrier, various telescopes and surveys have been designed to be sensitive to low surface brightness emission, making use of specialized algorithms and instruments to detect/characterize low-luminosity galaxies (e.g., Greco et al. 2018; van Dokkum et al. 2020). As a result, wide-field surveys are now providing comprehensive catalogs of low-luminosity galaxies.

Past studies of star formation in dwarf galaxies have been subject to these same limitations. For instance, while Geha et al. (2012) were able to study complete samples of galaxies with $M_* \gtrsim 10^8\ M_\odot$ with Sloan Digital Sky Survey (SDSS) spectroscopy, they probe only a very small volume at lower masses. Galaxies with masses $M_* \lesssim 10^7\ M_\odot$ have not yet been exhaustively analyzed.

The interpretation of detected low surface brightness objects generally requires ancillary data, such as spectroscopy or high-resolution imaging (see, e.g., Greco et al. 2021). Archival data offer a shortcut: if dwarf galaxies are sought and found in fields that already have a suite of ancillary data, the task of determining distances, structural parameters, and stellar population parameters is far more efficient. Here we present the serendipitous identification of an isolated and seemingly quenched dwarf galaxy in the well-studied COSMOS-CANDELS field.

2. A Faint, Extended Object in the COSMOS Field

2.1. HST Observations

The COSMOS-CANDELS (Koekemoer et al. 2011; Grogin et al. 2011) field covers ∼200 square arcmin and is one of the most observed regions in the sky, with data taken in all major wavelength regimes from X-ray to radio.

COSMOS-dw1 ($\alpha = 10^{\rm h}00^{\rm m}30\overset{\rm s}{.}03$, $\delta = +02°08'59\overset{''}{.}47$) was identified in archival Hubble Space Telescope (HST) data of the COSMOS field as an object with a semiresolved appearance, suggesting that it is nearby. It is split in multiple very faint objects in standard catalogs (e.g., Alam et al. 2015), but was noted as nearby in Xi et al. (2018) based on a photometric redshift.

We obtained the CTE-corrected individual `flc` files in the ACS/WFC F475W, F606W, and F814W bands from the HST Archive. We use `DrizzlePac` (STSCI Development Team 2012) to align the images in each filter via `TweakReg`

[8] NASA Hubble Fellow.
[9] NSF Astronomy & Astrophysics Postdoctoral Fellow.

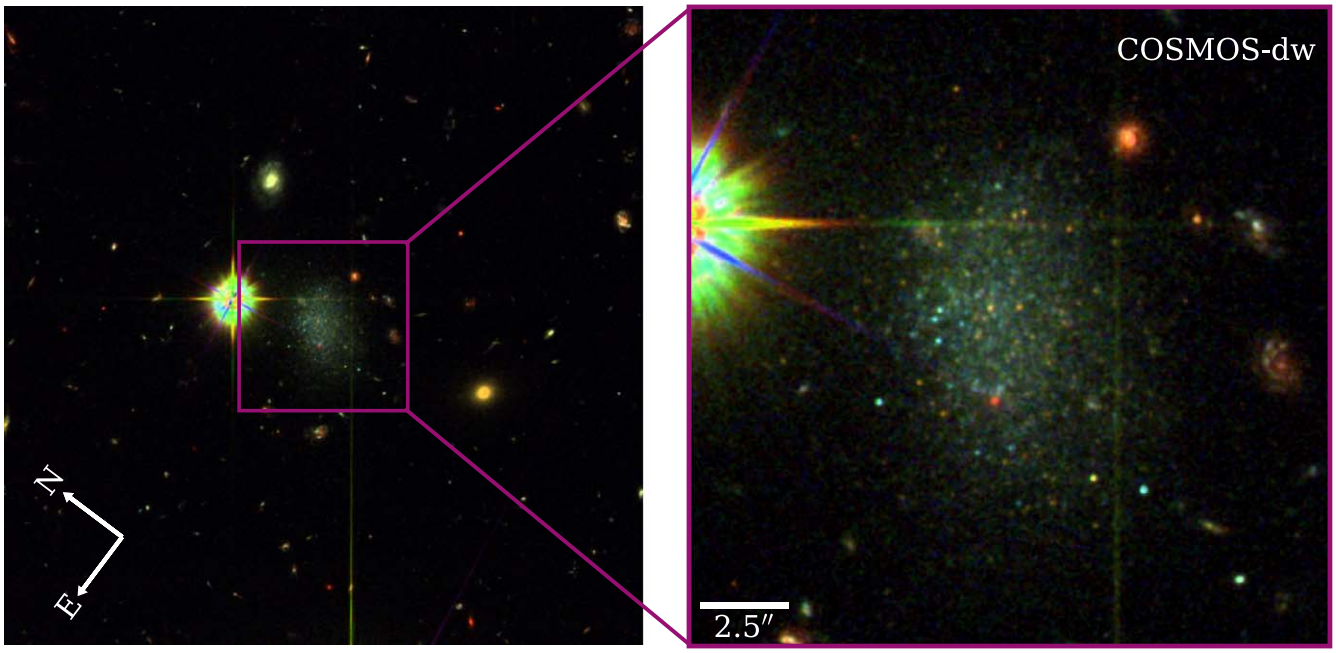

Figure 1. Both panels show color composite image of COSMOS-dw1 using F475W, F606W, and F814W. The left panel is 68″× 68″; the right panel is 18″ × 18″.

and then combine them via AstroDrizzle.[10] Total exposure times are 2028 s in F475W, 3328 s in F606W, and 6864 s in F814W.

A color composite image combining the HST data is shown in Figure 1. Several notable features are apparent. COSMOS-dw1 is a low surface brightness, semiresolved object. Its appearance is somewhat asymmetric, as it has a clump of blue stars off-center to the north. The rest of the galaxy appears to be dominated by red, likely post-main-sequence, stars that are distributed more evenly.

2.2. GALFIT

We begin by measuring the global structural parameters of the galaxy, such as its apparent size, brightness, and color, using GALFIT (Peng et al. 2010). We first ran GALFIT on the combined F814W+F606W image, after smoothing it with a Gaussian kernel with $\sigma = 2$ pix (0.″1). The galaxy was modeled with a single Sérsic fit and the image was aggressively masked, using a SEP (Bertin & Arnouts 1996; Barbary 2016) segmentation map and manually masking additional potential contaminants. The resulting Sérsic index is $n = 0.69$, and the effective radius is 4.″20. Next, GALFIT was run in each band separately, holding the $r_{\rm eff}$, Sérsic index, position angle, ellipticity, and x, y position fixed and letting only the brightness vary in the fit. The resultant parameters of our GALFIT runs are listed in Table 1. Errors are determined in the following way. Eleven copies of the best-fitting GALFIT model were injected into uncrowded areas in our images and then fitted in the same way as the actual data. The rms variation in the resulting parameters was taken as the uncertainty for each parameter. This method captures errors that are introduced by improper masking of background sources and noise. However, it assumes that the galaxy is smooth and has a perfect Sérsic profile, and it does not take deviations from those assumptions into account.

[10] We did not use existing data products from CANDELS or 3D-HST for consistency with our analysis of individual flc files in Section 4.

Table 1
COSMOS-dw1–Observed Properties

Parameter	Value
$m_{\rm F475W}$	19.43 ± 0.07
$m_{\rm F606W}$	19.31 ± 0.04
$m_{\rm F814W}$	19.17 ± 0.03
F475W−F814W	0.26 ± 0.08
F606W−F814W	0.14 ± 0.05
$\mu_{0,\,g}$ (mag arcsec^{-2})	23.03 ± 0.08
$\mu_{0,\,V}$ (mag arcsec^{-2})	22.90 ± 0.06
$\mu_{0,\,I}$ (mag arcsec^{-2})	22.77 ± 0.05
$\mu_{\rm eff,\,g}$ (mag arcsec^{-2})	24.19 ± 0.08
$\mu_{{\rm eff},V}$ (mag arcsec^{-2})	24.07 ± 0.06
$\mu_{{\rm eff},I}$ (mag arcsec^{-2})	23.93 ± 0.05
Sérsic index	0.69 ± 0.01
b/a	0.721 ± 0.008
PA (deg)	-30.2 ± 0.6
$r_{\rm eff}$ (arcsec)	4.20 ± 0.07
$R_{\rm eff}$ (kpc)	0.45 ± 0.06
$v_{\rm rad}$ (km s^{-1})	1222 ± 64
$D_{\rm SBF}$ (Mpc)	22 ± 3

Note. Intrinsic parameters are calculated assuming a distance of 22 Mpc. All magnitudes are quoted in the AB system.

3. Velocity and Distance

3.1. Keck Spectroscopy

We observed COSMOS-dw1 with the Low Resolution Imaging Spectrograph (LRIS; Oke et al. 1995) on Keck I on 2018 November 5. The 1.″5 long slit was used, with the 300 l mm^{-1} grism blazed at 5000 Å. The total exposure time was 4600 s in excellent conditions. The data reduction followed standard procedures for long-slit data. The spectrum is shown

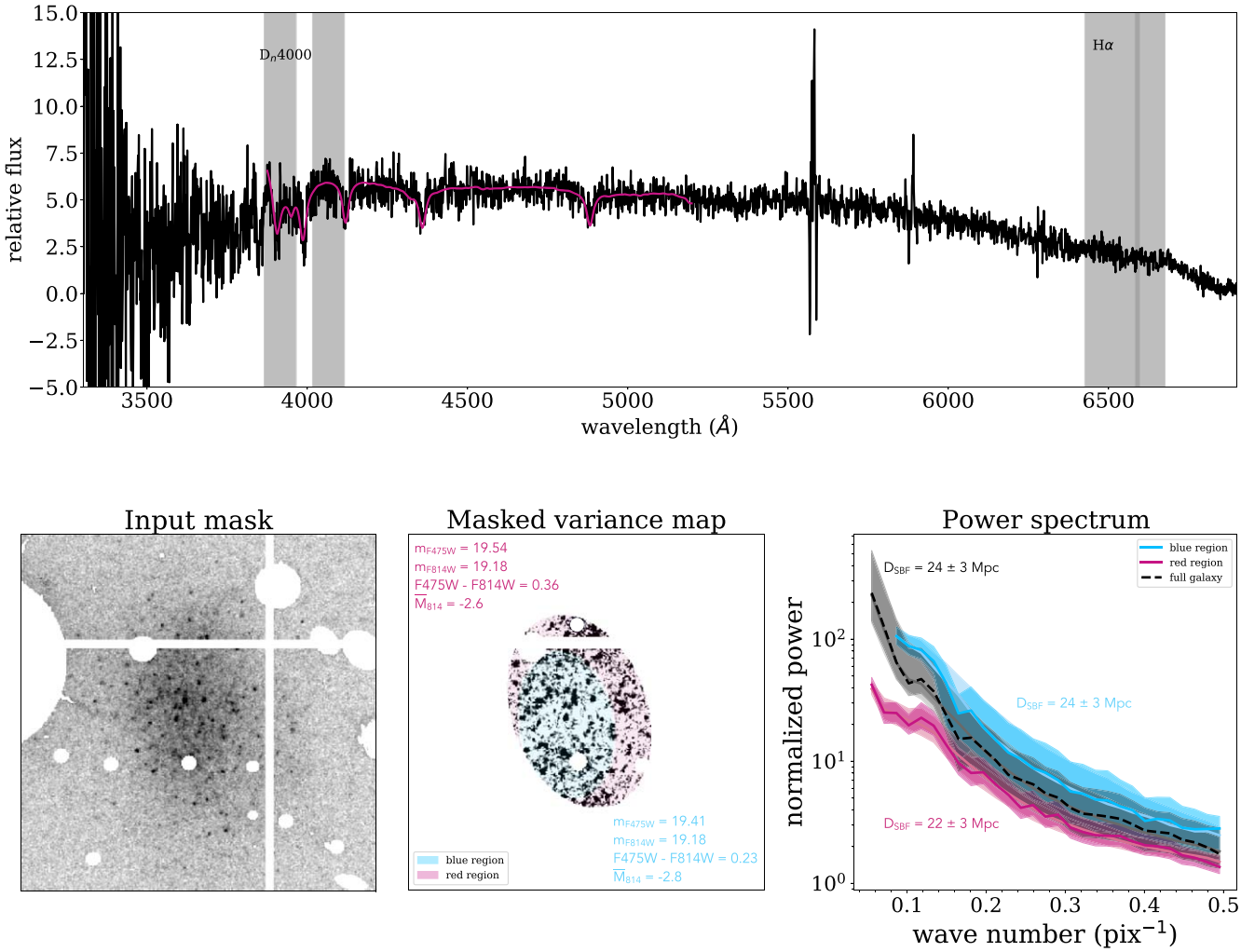

Figure 2. Top panel: the median model spectrum (a linear combination of weighted template spectra) $\pm 1\sigma$ output by `emcee` (Foreman-Mackey et al. 2013) is shown in pink, plotted over a subset of our LRIS data on the interval 3875–5200 Å. In black, we show the flux-calibrated spectrum (the instrument response curve was from a different night). Gray regions mark the continuum around the 4000 Å break, used to calculate D_n4000, and the Hα line, used to determine the rms error on the equivalent width. Bottom panel: at the left, we show the masked combined F814W image used for the full galaxy SBF analysis (also used when running `GALFIT`). The middle panel shows the variance map of the full galaxy (as well as the red and blue regions that were analyzed). The median of the fits to the power spectra are shown at the right, with the shaded area representing the 68th percentile of the distribution, plotted under the median measured power spectra and the 68th percentile of their distributions.

in Figure 2. The most prominent features are strong Balmer absorption lines, indicating a dominant population of A stars and an age of ∼1 Gyr. There are no clearly detected emission lines.

We use a χ^2 minimization scheme over the spectral range 3875–5200 Å to determine the radial velocity, with `Flexible Stellar Population Synthesis` (`FSPS`; Conroy et al. 2009) template spectra smoothed to the instrumental resolution. We measure a heliocentric radial velocity of 1222 ± 64 km s^{-1}; the uncertainty in this result includes fits for a range of ages (0.5–8 Gyr) and metallicities ($-2 \leqslant$ [Fe/H] $\leqslant -1$).

This velocity is consistent with COSMOS-dw1 being at a distance of $20.0^{+0.8}_{-0.7}$ Mpc via the `Cosmicflows-3` (Kourkchi et al. 2020; $H_0 = 75$ km s^{-1} Mpc^{-1}, $\Omega_M = 0.27$, and $\Omega_\Lambda = 0.73$) calculator. However, this uncertainty ignores the peculiar velocity of COSMOS-dw1; a peculiar velocity of 300 km s^{-1} would correspond to a distance uncertainty of 5 Mpc.

3.2. Surface Brightness Fluctuations

A distance can also be obtained from the HST imaging. The galaxy is only semiresolved, and we cannot obtain a distance from the tip of the red giant branch (see Section 4.3). Instead we use surface brightness fluctuations (SBFs; e.g., Tonry & Schneider 1988; Greco et al. 2021) to constrain the distance to COSMOS-dw1. The SBF method relies on the decreasing pixel-to-pixel brightness variance of a stellar population with increasing distance.

Because this method is sensitive to the nature of the stellar population, we use the integrated galaxy colors shown in Table 1 and the $\bar{M}_{814}$ versus g_{475}–I_{814} relation from Carlsten et al. (2019). We find $\bar{M}_{814} = -2.8 \pm 0.3$ using the luminosity-weighted average g_{475}–I_{814} color of the galaxy (see Table 1).

We then generate a variance map from our raw F814W image and the model returned from `GALFIT` ([image–model]/$\sqrt{\text{model}}$), which we mask, using the aggressive mask we applied to our `GALFIT` runs plus an elliptical aperture to make

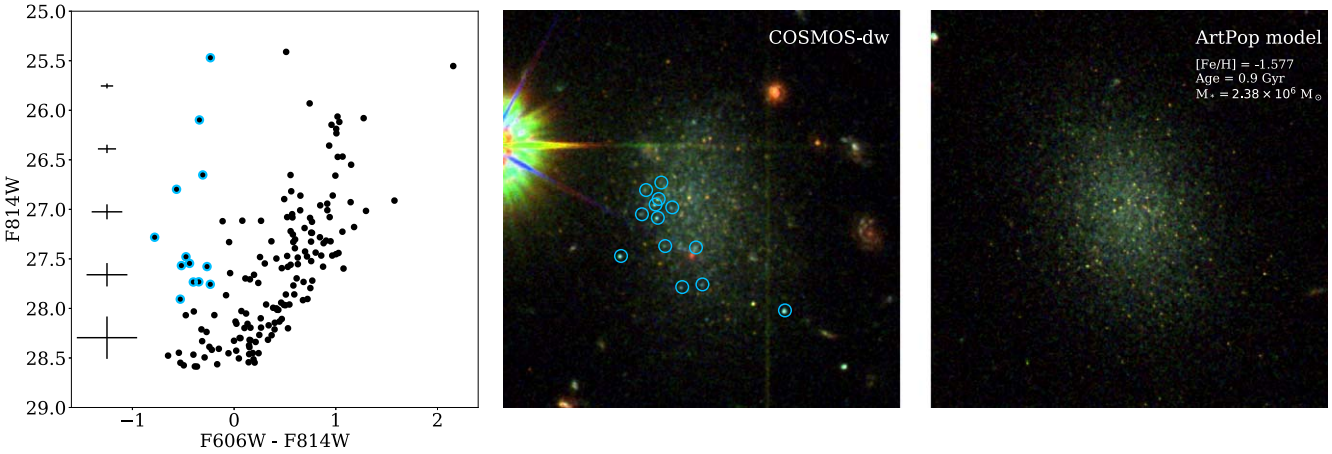

Figure 3. Left panel: COSMOS-dw1's CMD is shown using stellar photometry from DOLPHOT. Average error bars for each m_{F814W} bin are shown at the far left. The points marked by a blue circle correspond to the brightest, bluest stars with F606W–F814W $\leqslant -0.2$ and $m_{F814W} \leqslant -28$. These same stars are marked in the RGB image of COSMOS-dw1 in the middle panel. Right panel: an ArtPop model of a simple stellar population placed at 22 Mpc that has the same integrated properties as COSMOS-dw1 (see Table 1).

sure any measured surface brightness fluctuations are actually coming from the galaxy. In order to avoid biasing our results with selection of aperture size (or the range of assessed wavenumbers), we run our SBF analysis repeatedly, randomly selecting our wavenumber range and ellipse dimensions from reasonable uniform distributions, storing the apparent SBF magnitude from each run.

As shown in Section 4.3 the galaxy has a region that is dominated by blue stars. We therefore separately analyze the blue region and red region (in addition to the full galaxy). As is evident from the power spectra (see Figure 2), the full galaxy measurement is strongly affected by the bright, resolved blue stars. As SBF is a more robust method within the redder regime, we adopt the measurement from our red region, finding that the galaxy is located at 22 ± 3 Mpc ($\bar{M}_{814} = -2.6 \pm 0.3$ and $\bar{m}_{814} = 29.15 \pm 0.08$), consistent with the redshift distance, which suggests this galaxy has a small peculiar velocity. The results from the full galaxy/blue region fall within these error bars (24 ± 3 Mpc), and the measurements for each subset of the galaxy are also consistent with the SBF distance using an extrapolation of the Blakeslee et al. (2010) relation.

We determine distance-dependent quantities with $D_{\rm SBF}$ (see Table 1). We find that the galaxy has a luminosity of $L_{\rm F606W} = (7 \pm 2) \times 10^6\ L_\odot$ and a physical size of $R_{\rm eff} = 450 \pm 60$ pc.

4. Stellar Population

4.1. Constraints from the Integrated Colors

We first use the HST-measured colors to constrain the stellar population properties. To break the age–metallicity degeneracy we assume that COSMOS-dw1 falls on the mass–metallicity relation. Running a grid of ages and metallicities through FSPS, COSMOS-dw1's integrated F606W−F814W and F475W−F814W colors and absolute F606W magnitude imply a stellar population of age 0.9 Gyr, [Fe/H] $= -1.6$, and $M_* = 2.4 \times 10^6\, M_\odot$. This age is qualitatively consistent with the prominent Balmer lines in the spectrum.

To illustrate that this simple stellar population (SSP) provides a reasonable description of the galaxy we use the ArtPop code (first described in Danieli et al. 2018; J. Greco and S. Danieli 2021, in preparation), which creates full 2D models of galaxies by drawing stars from isochrones. We then inject the simulated galaxy into our drizzled HST images on a filter-by-filter basis (see the right panel of Figure 3). The overall appearance is a good match, although the morphological structure of the model is clearly more regular than that of the data. Furthermore, there are blue stars that are not accounted for in the ArtPop model; we will return to those below.

4.2. Constraints from Spectral Indices

We measure EW(Hα) and the strength of the 4000 Å line break (Balogh et al. 1999). We find an equivalent width consistent with no Hα emission (-0.4 ± 0.5 Å) and D_n4000 index $= 1.22 \pm 0.02$, which is *just* inconsistent with a quenched galaxy per the relation and criterion from Geha et al. (2012). The Hα equivalent width corresponds to a 3σ specific star formation rate (sSFR) upper limit of $1.5 \times 10^{-12}\ {\rm yr}^{-1}$ (Belfiore et al. 2018). We infer that the galaxy is young but is not forming stars at present.

4.3. Evidence for a Complex Stellar Population

We use the ACS module from DOLPHOT, an adapted version of HSTphot (Dolphin 2000), to obtain photometry of individual stars in COSMOS-dw1. We follow the module's preprocessing steps, including bad pixel rejection, sky estimation, and fine alignment of the input images. Using our drizzled F814W image as the reference, we run DOLPHOT twice, once for all F814W and F606W flc files and once for F814W and F475W. For the photometry's point-spread function (PSF) fitting, we use TinyTim PSFs (Krist et al. 2011).

Our parameter files closely follow the recommendations from the DOLPHOT handbook, but we adopt the Dalcanton et al. (2009) values for the sky-fitting parameter (*FitSky* = 3), aperture radius (*RAper* = 10 pix), and flag that forces all detected sources to be treated like stars for the purpose of fitting (*Force1* = 1).

We make quality cuts on the detected/photometered sources in the DOLPHOT output to make sure we only include sources with high-quality stellar photometry. Following Danieli et al. (2017), we include "good stars" (*object type* = 1) with high-quality photometry (photometry quality flag $\leqslant$2), high signal-to-noise (S/N $\geqslant 4$), and object sharpness within a star-like

range ($-0.3 \leqslant \mathrm{sharpness}_{\mathrm{F606W+F814W}} \leqslant 0.75$). Spatially, we include all stars that reasonably belong to COSMOS-dw1. The resultant color–magnitude diagram (CMD) is shown in the left panel of Figure 3.

As is notable in the color composite images of COSMOS-dw1, the CMD shows a population of bright, very blue stars. These stars (F606W−F814W $\leqslant -0.2$ and $m_{\mathrm{F814W}} \leqslant -28$) are marked in both the CMD and the RGB image in Figure 3. Their location provides an upper limit to their age: the dynamical time at their distance from the center is only $\approx 10^8$ yr, and the stars would have dispersed throughout the galaxy if they formed earlier than that.

5. Environment

Dwarf galaxies are thought to be quenched predominantly by environmental effects, such as ram pressure stripping and tidal stripping (e.g., Boselli & Gavazzi 2006; Weisz et al. 2011b; Fillingham et al. 2018), so it is expected that seemingly quiescent galaxies with little-to-no evidence of Hα emission are within one to two virial radii of a bright companion. Intriguingly, COSMOS-dw1 does not have an obvious luminous companion.

We search within 5° (∼2 Mpc projected at 22 Mpc) and 300 km s^{-1} of COSMOS-dw1 in order to assess its immediate environment. There are 19 nearby galaxies within this projected distance in the radial-velocity range 922–1522 km s^{-1}. Assuming each of these nearby galaxies is also located at a distance of 22 Mpc and using an r-band mass-to-light ratio of $\Upsilon_r = 3.05\, M_\odot L_\odot^{-1}$ (Bell et al. 2003), we find that 2 of the 19 galaxies exceed the minimum mass to potentially be considered a "luminous neighbor" ($M_\star > 2.5 \times 10^{10}\, M_\odot$) as in Geha et al. (2012). The closest of these, NGC 3166, is 1.4 Mpc away in projection, just inside the 1.5 Mpc limit used by Geha et al. (2012) [11]

We further explore an association with this galaxy, or other nearby galaxies, by estimating the virial radii of potential neighbors using the stellar mass–r_{80} and r_{80}–virial radius relations defined in Mowla et al. (2019), which take $\mathbf{\Delta}_c = 200$. The results are shown in Figure 4. NGC 3044, the closest non-dwarf galaxy to COSMOS-dw1 with a calculated stellar mass below our luminous neighbor threshold ($M_* \sim 1.2 \times 10^{10}\, M_\odot$) and $v_{\mathrm{rad}} - v_{\mathrm{rad,dw}} = 66$ km s^{-1}, is located $4.1 R_{\mathrm{vir}}$ from our isolated dwarf in projection. NGC 3166, the closest luminous neighbor ($M_* \sim 6.1 \times 10^{10}\, M_\odot$, $\mathbf{\Delta} v_{\mathrm{rad}} = 106$ km s^{-1}), is $3.9 R_{\mathrm{vir}}$ away. It is worth noting that these values are strict lower limits, as we assume that the projected distances equal the physical distances.

There are also three dwarf galaxies near COSMOS-dw1: LEDA 1230703 ($M_* = 1.2 \times 10^8\, M_\odot$, $\mathbf{\Delta} v_{\mathrm{rad}} = -109$ km s^{-1}), 0.41 Mpc ($5.3 R_{\mathrm{vir}}$) from COSMOS-dw1; 2dFGRS TGN353Z197 ($M_* = 8.3 \times 10^7\, M_\odot$, $\mathbf{\Delta} v_{\mathrm{rad}} = 124$ km s^{-1}) at a distance of 0.48 Mpc ($6.7 R_{\mathrm{vir}}$); and SDSS J100517.67+013831.2 ($M_* = 8.3 \times 10^7\, M_\odot$, $\mathbf{\Delta} v_{\mathrm{rad}} = 43$ km s^{-1}), 0.50 Mpc ($6.9 R_{\mathrm{vir}}$) from COSMOS-dw1.

We note that the nearest galaxies' $\mathbf{\Delta} v_{rad}$ distribution is consistent with the distribution of the full sample returned in our search.

[11] We note that the intriguing early-type galaxy Ark 227 (Arakelian 1975) is at a projected distance of only 4 arcmin from COSMOS-dw1. However, its redshift ($cz = 1793$ km s^{-1}; Falco et al. 1999) is 571 km s^{-1} removed from that of COSMOS-dw1, corresponding to a distance of approximately 30 Mpc and effectively ruling out an association.

6. Discussion and Conclusion

We report the serendipitous identification of an isolated quenched low-mass galaxy at a distance of ∼22 Mpc. All other known and well-studied galaxies in this region of parameter space are in the immediate vicinity of the Local Group. The four isolated Local Group dwarfs are Cetus (Whiting et al. 1999), Tucana (Lavery 1990), KKR 25 (Makarov et al. 2012), and KKs 3 (Karachentsev et al. 2015). There is evidence to suggest that Cetus and Tucana are backsplash galaxies (Teyssier et al. 2012), which were environmentally quenched during a previous passage through the Local Group. KKR 25 and KKs 3 are ≈2 Mpc away from the Local Group, farther than the projected distance of COSMOS-dw1 to its nearest potential neighbor. However, NGC 3166 and NGC 3044 have a lower mass than the Milky Way and M31, and when expressed in virial radii, KKR 25 and KKS 3 are a factor of ≈2 *closer* to their nearest neighbor than COSMOS-dw1 is.

The quenching mechanism for COSMOS-dw1 is a puzzle. The isolation of the galaxy combined with the fact that quenching happened recently makes an environmental cause very unlikely. Interestingly, all three galaxies (COSMOS-dw1, KKR 25, and KKS 3) have complex stellar populations (Makarov et al. 2012; Karachentsev et al. 2015), suggesting that star formation stopped and started several times over their lifetimes.

We suggest that quenching was due to internal feedback. Simulations suggest that supernova feedback can shut down star formation in low-mass galaxies, but only for a short time (Fitts et al. 2017; Fillingham et al. 2018). Whenever we catch a galaxy in this short-lived phase we observe it to be young. Of the three galaxies in this limited sample, COSMOS-dw1 appears to be the youngest, and the clump of blue stars in COSMOS-dw1 may represent the site of the feedback event that temporarily halted further star formation (see also Geha et al. 2012). The intriguing nearby spheroidal object APPLES 1 (Pasquali et al. 2005) may also fit in this category: its distance is uncertain, but its young age and likely isolation are consistent with recent quenching.

In the near future, various wide-field surveys/instruments such as the Rubin Observatory's Legacy Survey of Space and Time (Ivezić et al. 2019) and, later, the Roman Space Telescope (Spergel et al. 2015) should help us determine how common these quiescent isolated dwarfs are. The fact that COSMOS-dw1 was found in a very small and very well-studied field suggests that they may be quite common (as indicated by Klypin et al. 2015) and can easily be missed. Low surface brightness-optimized surveys, such as the HSC-SSP (Aihara et al. 2018) and the Dragonfly Wide Field Survey (Danieli et al. 2020), will provide an additional avenue to obtaining a census of isolated low-mass quiescent galaxies.

The authors would like to thank the anonymous referee for comments and suggestions that significantly improved the manuscript, as well as Dong Dong Shi and Xian Zhong Zheng for the initial identification of this galaxy. S.D. is supported by NASA through Hubble Fellowship grant HST-HF2-51454.001-A awarded by the Space Telescope Science Institute, which is operated by the Association of Universities for Research in Astronomy, Incorporated, under NASA contract NAS5-26555. A.J.R. was supported as a Research Corporation for Science Advancement Cottrell Scholar.

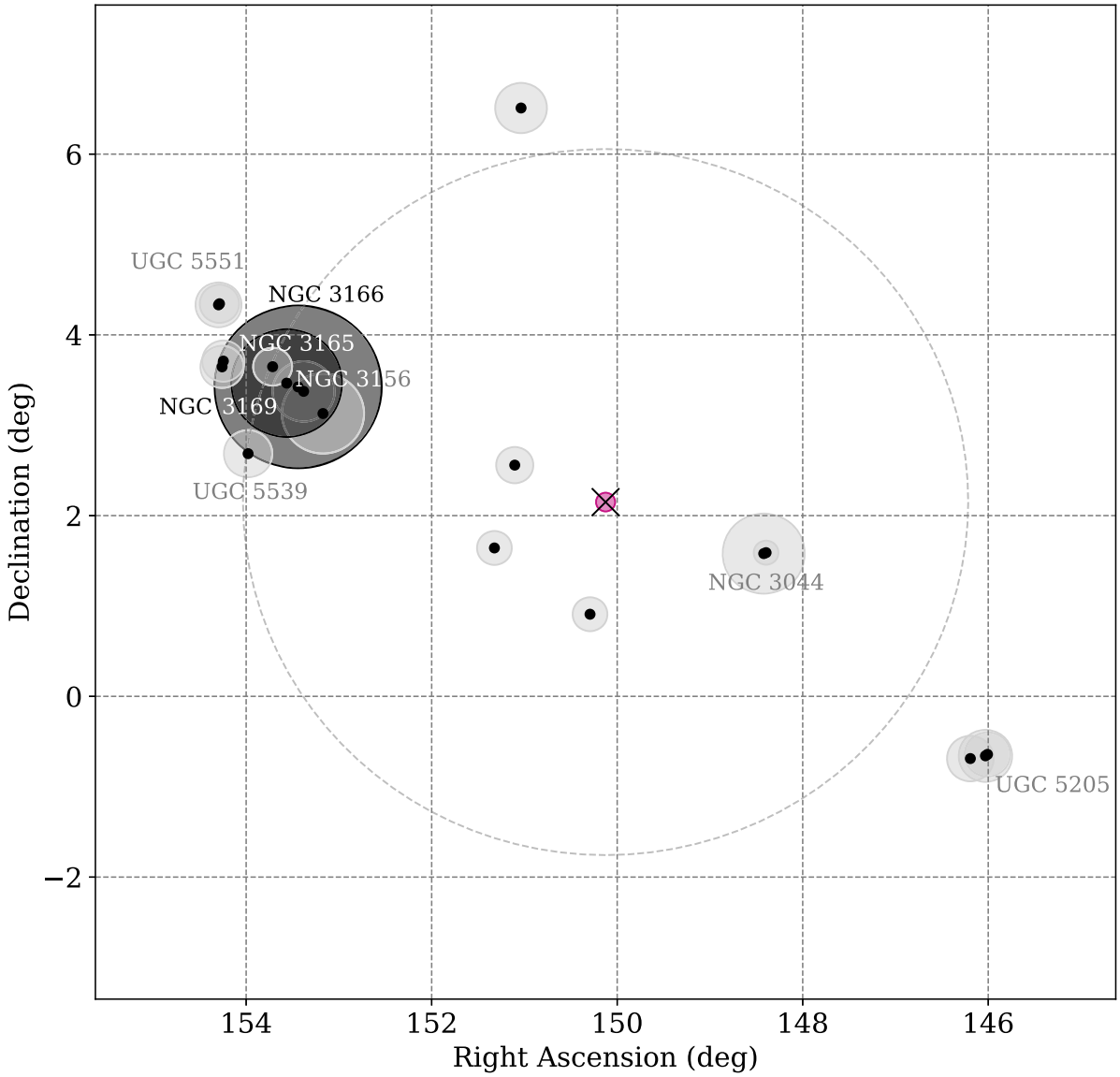

Figure 4. We assess the environment of COSMOS-dw1 by estimating the virial radii of nearby galaxies, assuming that they are all at the same distance as the dwarf. We show the 1.5 Mpc projected radius as the dashed gray circle, while all galaxies within 5° and 300 km s^{-1} of COSMOS-dw1 are shown as black points with their virial radii underplotted; galaxies with $M_* > 2.5 \times 10^{10}\ M_\odot$ are marked by darker underplotted virial radii. NGC and UGC objects are labeled. Each square of the grid is 0.77 × 0.77 Mpc^2 at a projected distance of 22 Mpc. We find that COSMOS-dw1 is at least $\gtrsim$4 virial radii away from any other galaxy.

ORCID iDs

Ava Polzin https://orcid.org/0000-0002-5283-933X
Pieter van Dokkum https://orcid.org/0000-0002-8282-9888
Shany Danieli https://orcid.org/0000-0002-1841-2252
Johnny P. Greco https://orcid.org/0000-0003-4970-2874
Aaron J. Romanowsky https://orcid.org/0000-0003-2473-0369

References

Aihara, H., Arimoto, N., Armstrong, R., et al. 2018, PASJ, 70, S4
Alam, S., Albareti, F. D., Allende Prieto, C., et al. 2015, ApJS, 219, 12
Arakelian, M. A. 1975, CoBAO, 47, 3
Balogh, M. L., Morris, S. L., Yee, H. K. C., Carlberg, R. G., & Ellingson, E. 1999, ApJ, 527, 54
Barbary, K. 2016, JOSS, 1, 58
Belfiore, F., Maiolino, R., Bundy, K., et al. 2018, MNRAS, 477, 3014
Bell, E. F., McIntosh, D. H., Katz, N., & Weinberg, M. D. 2003, ApJS, 149, 289
Bertin, E., & Arnouts, S. 1996, A&AS, 117, 393
Blakeslee, J. P., Cantiello, M., Mei, S., et al. 2010, ApJ, 724, 657
Boselli, A., & Gavazzi, G. 2006, PASP, 118, 517
Carlsten, S. G., Beaton, R. L., Greco, J. P., & Greene, J. E. 2019, ApJ, 879, 13
Conroy, C., Gunn, J. E., & White, M. 2009, ApJ, 699, 486
Dalcanton, J. J., Williams, B. F., Seth, A. C., et al. 2009, ApJS, 183, 67
Danieli, S., van Dokkum, P., & Conroy, C. 2018, ApJ, 856, 69
Danieli, S., van Dokkum, P., Merritt, A., et al. 2017, ApJ, 837, 136
Danieli, S., Lokhorst, D., Zhang, J., et al. 2020, ApJ, 894, 119
Dolphin, A. E. 2000, PASP, 112, 1383
Falco, E. E., Kurtz, M. J., Geller, M. J., et al. 1999, PASP, 111, 438
Fillingham, S. P., Cooper, M. C., Boylan-Kolchin, M., et al. 2018, MNRAS, 477, 4491
Fitts, A., Boylan-Kolchin, M., Elbert, O. D., et al. 2017, MNRAS, 471, 3547
Foreman-Mackey, D., Hogg, D. W., Lang, D., & Goodman, J. 2013, PASP, 125, 306
Geha, M., Blanton, M. R., Yan, R., & Tinker, J. L. 2012, ApJ, 757, 85
Greco, J. P., van Dokkum, P., Danieli, S., Carlsten, S. G., & Conroy, C. 2021, ApJ, 908, 24
Greco, J. P., Greene, J. E., Strauss, M. A., et al. 2018, ApJ, 857, 104
Grogin, N. A., Kocevski, D. D., Faber, S. M., et al. 2011, ApJS, 197, 35

Ivezić, Ž., Kahn, S. M., Tyson, J. A., et al. 2019, ApJ, 873, 111
Karachentsev, I. D., Makarova, L. N., Makarov, D. I., Tully, R. B., & Rizzi, L. 2015, MNRAS, 447, L85
Klypin, A., Karachentsev, I., Makarov, D., & Nasonova, O. 2015, MNRAS, 454, 1798
Koekemoer, A. M., Faber, S. M., Ferguson, H. C., et al. 2011, ApJS, 197, 36
Kourkchi, E., Courtois, H. M., Graziani, R., et al. 2020, AJ, 159, 67
Krist, J. E., Hook, R. N., & Stoehr, F. 2011, Proc. SPIE, 8127, 81270J
Lavery, R. J. 1990, IAUC, 5139, 2
Makarov, D., Makarova, L., Sharina, M., et al. 2012, MNRAS, 425, 709
Mateo, M. L. 1998, ARA&A, 36, 435
Mowla, L., van der Wel, A., van Dokkum, P., & Miller, T. B. 2019, ApJL, 872, L13
Oke, J. B., Cohen, J. G., Carr, M., et al. 1995, PASP, 107, 375
Pasquali, A., Larsen, S., Ferreras, I., et al. 2005, AJ, 129, 148
Peng, C. Y., Ho, L. C., Impey, C. D., & Rix, H.-W. 2010, AJ, 139, 2097
Simon, J. D. 2019, ARA&A, 57, 375
Spergel, D., Gehrels, N., Baltay, C., et al. 2015, arXiv:1503.03757
STSCI Development Team 2012, DrizzlePac: HST image software, Astrophysics Source Code Library, ascl:1212.011
Teyssier, M., Johnston, K. V., & Kuhlen, M. 2012, MNRAS, 426, 1808
Tollerud, E. J., Bullock, J. S., Strigari, L. E., & Willman, B. 2008, ApJ, 688, 277
Tonry, J., & Schneider, D. P. 1988, AJ, 96, 807
van Dokkum, P., Lokhorst, D., Danieli, S., et al. 2020, PASP, 132, 074503
Walsh, S. M., Willman, B., & Jerjen, H. 2009, AJ, 137, 450
Weisz, D. R., Dolphin, A. E., Dalcanton, J. J., et al. 2011a, ApJ, 743, 8
Weisz, D. R., Dalcanton, J. J., Williams, B. F., et al. 2011b, ApJ, 739, 5
Whiting, A. B., Hau, G. K. T., & Irwin, M. 1999, AJ, 118, 2767
Xi, C., Taylor, J. E., Massey, R. J., et al. 2018, MNRAS, 478, 5336